ICWE14
June 21-26, 2015 | Porto Alegre - Brazil
14th INTERNATIONAL CONFERENCE ON WIND ENGINEERING

Modelling the interaction of VIV and galloping for rectangular cylinders

Claudio Mannini[1], Tommaso Massai[1], Antonino M. Marra[1], Gianni Bartoli[1]
[1]CRIACIV/ Department of Civil and Environmental Engineering, University of Florence, Florence, Italy
email: claudio.mannini@dicea.unifi.it, tmassai@dicea.unifi.it, antonino.marra@dicea.unifi.it, gianni.bartoli@unifi.it

ABSTRACT: Several bluff bodies, such as rectangular cylinders with moderate side ratio, in particular conditions of mass and damping of the mechanical system can experience the interaction of vortex-induced vibration (VIV) and galloping, giving rise to an instability with peculiar features. Two analytical models are available in literature to simulate this phenomenon and they were tested so far only in the case of a square cylinder. Both models rely on the linear superposition of the unsteady forces producing vortex-induced vibration, obtained through nonlinear wake-oscillator models, and the quasi-steady forces that are responsible for galloping. These models are reviewed here and they are tested in the case of a rectangular 3:2 cylinder, which showed a strong proclivity to VIV-galloping interference and for which the authors carried out a large number of experimental tests. An extensive sensitivity study on the parameters appearing in the equations of the two models was carried out to better understand their actual behavior and their potentialities. Despite the theoretical limits, these models are able to reproduce some interesting features of the complex phenomenon of interaction observed in the wind tunnel tests. In particular, Tamura and Shimada's model seems to be able to reproduce the nearly linear increase of the oscillation amplitude for wind speeds higher than the Kármán-vortex resonance velocity, if a key parameter in the equations is suitably set. Therefore, a future effort to further explore and improve this model is doubtless worth.

KEY WORDS: Galloping; Vortex-Induced Vibrations; Rectangular cylinders; Analytical models.

1 INTRODUCTION

The interaction of vortex-induced vibration (VIV) and galloping can occur for several bluff bodies and in particular for rectangular cylinders with moderate side ratio. The authors in some previous works [1-3] presented a review and an experimental investigation on this phenomenon. Typically, VIV is a low reduced wind speed and galloping a high reduced wind speed flow-induced vibration. Nevertheless, in case of interference between the two phenomena, instead of the expected separated ranges of excitation, a galloping-type instability (*i.e.*, velocity unrestricted) starts at the theoretical critical wind speed for VIV (*i.e.*, at the Kármán-vortex resonance wind speed). The difference between VIV-galloping interference and classical behavior is sketched in Figure 1.

This instability is not only physically interesting but also very important from the practical engineering point of view, as it implies large-amplitude oscillations where they are not predicted by the classical theories for VIV and galloping. Consequently, a model for the interaction of the two phenomena would be a precious tool for the engineers but it represents a challenging task, being the underlying physics of interference not fully understood yet. For this reason, only few attempts to provide a mathematical model are found in the literature.

To the writers' knowledge, the first model was proposed by Santosham [4], who simply added a harmonic force at the Strouhal frequency to the quasi-steady self-excited forces. The model predicted the delay of galloping due to vortex shedding in water ("asynchronous quenching") but failed to predict any significant interaction in air. In the 70s, Bouclin [5] proposed a more advanced model and applied it to the case of a square cylinder. Some years later, Corless and Parkinson [6] slightly modified this model and solved the equation with the method of multiple scales. In the same period, Tamura and Shimada [7] presented an alternative model for the interference of VIV and galloping and applied it again to the case of a square cylinder.

In the analysis to follow, the most interesting models available in literature, that is Corless and Parkinson's and Tamura and Shimada's models, are reconsidered for the case of a rectangular cylinder with a side ratio $B/D = 1.5$, being B and D respectively the streamwise and cross-flow section dimensions, placed perpendicularly to the smooth airflow with zero angle of attack (see Figure 2). The experimental analyses conducted by the authors [1-3] showed that this cross section is highly prone to the interference of VIV and galloping. The results of the classical quasi-steady theory for galloping [8-9] were shown too. In the paper, particular attention is devoted to the discussion of the model parameters and extensive sensitivity studies are carried out.

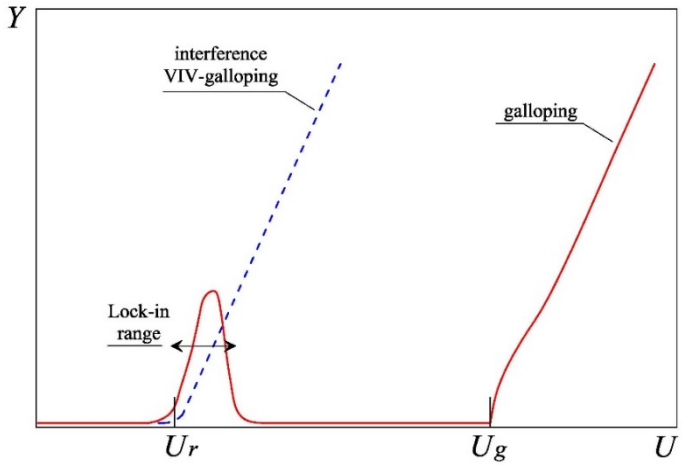

Figure 1. Comparison between classical behavior with separated VIV and galloping excitations (solid line) and instability due to the interference between the two phenomena (dashed line).

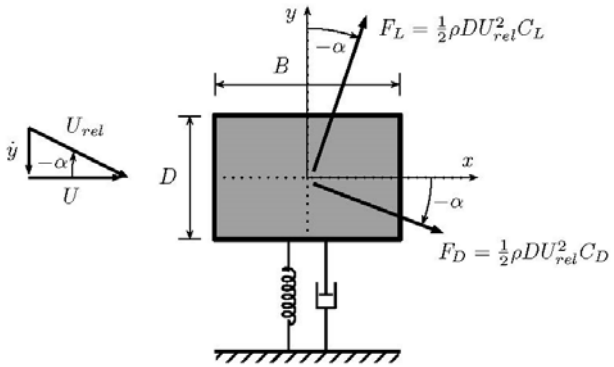

Figure 2. Evaluation of the transverse force on a vibrating rectangular cylinder with the quasi-steady approach. U_{rel} denotes the apparent flow speed due to the body displacement velocity.

2 QUASI-STEADY MODEL FOR GALLOPING

According to the quasi-steady theory [8-9], the forces exerted by the flow on an oscillating body can be calculated at each time instant as if the body was stationary and invested by the apparent steady flow, as shown in Figure 2. Therefore, the transverse force coefficient acting on a slender prismatic structure can be calculated as follows:

$$C_{Fy}(\alpha) = sec(\alpha)\cdot\left[C_L(\alpha) + C_D(\alpha)\cdot tg(\alpha)\right] \tag{1}$$

where

$$\alpha = -arctg\left(\frac{\dot{y}}{U}\right) = -arctg\left(\frac{Y'}{V_{red}}\right) \tag{2}$$

being $Y = y/D$ is the nondimensional amplitude of vibration; $V_{red} = U/2\pi n_0 D$ the reduced velocity, n_0 the system still-air natural frequency, U the undisturbed flow speed; $(\cdot)'$ denotes differentiation with respect to nondimensional time $\tau = 2\pi n_0 t$, where t is the physical time.

By introducing a polynomial approximation of the transverse force (with coefficients A_1, A_3, …), it is possible to write:

$$C_{Fy} \cong A_1\frac{Y'}{V_{red}} + A_3\left(\frac{Y'}{V_{red}}\right)^3 + \ldots \tag{3}$$

Finally, introducing it in the equation of motion of a linear oscillator, one obtains:

$$Y'' + 2\zeta_0 Y' + Y = m^* V_{red}^2\left[A_1\frac{Y'}{V_{red}} + A_3\left(\frac{Y'}{V_{red}}\right)^3 + \ldots\right] \tag{4}$$

where ζ_0 is the ratio-to-critical damping coefficient, $m^* = \rho D^2/2m$ the mass ratio, m the mass of the cylinder per unit length and ρ the air density. The quasi-steady galloping response of an elongated prismatic body can be predicted through this equation.

3 MODELS FOR VIV-GALLOPING INTERACTION

3.1 Corless and Parkinson's model

In 1977, Bouclin [5] proposed a model where the total transverse force exciting the body oscillator is given by the linear superposition of the quasi-steady transverse force in the polynomial form proposed by Parkinson [8] (Eq. 3) and the unsteady force due to vortex excitation according to the Hartlen and Currie model [10]. The latter utilizes a Rayleigh differential equation for the lift force coefficient coupled to the mechanical oscillator to account for the self-limiting behavior of VIV oscillations. The nonlinear term is calibrated in order to retrieve the measured fluctuating lift coefficient when the motion amplitude tends to zero. The lift force is taken, rather arbitrarily, to be proportional to the transverse velocity of the oscillating body. Bouclin [5] numerically solved the nonlinear system of ordinary differential equations for a square cylinder in a water flow. Several features of the interaction phenomenon were captured by the model, such as the instability onset at the Kármán-vortex resonance velocity or the delay of galloping due to vortex shedding ("quenching") when the galloping critical flow speed calculated with the quasi-steady theory, U_g, is lower than the Kármán-vortex resonance flow speed U_r. By contrast, the model failed to reproduce the secondary resonance at $U_r/3$ observed in the experiments for low structural damping.

In 1988, Corless and Parkinson [6] slightly modified and generalized the model, in particular by adding an inertial coupling term. The resulting system of nonlinear differential equations then becomes:

$$Y'' + 2\zeta_0 Y' + Y = m^* V_{red}^2 C_v + m^* V_{red}^2 \left[A_1 \frac{Y'}{V_{red}} + A_3 \left(\frac{Y'}{V_{red}} \right)^3 + \dots \right] \tag{5}$$

$$C_v'' - a \cdot \upsilon \cdot C_v' \cdot \left(1 - \frac{4}{3\upsilon^2 C_{L0}^2} C_v'^2 \right) + \upsilon^2 C_v = \frac{b}{\upsilon^2} Y'' + \frac{c}{\upsilon} Y' \tag{6}$$

where C_v denotes the unsteady lift force due to vortex excitation. $\upsilon = 2\pi \cdot St \cdot V_{red} = U/U_r$ is the velocity ratio with respect to the Kármán-vortex resonance, St the Strouhal number, U and $U_r = n_0 D/St$ respectively the undisturbed and the Kármán-vortex resonance flow speeds. C_{L0} is the amplitude of the lift coefficient fluctuation for the stationary cylinder, while a, b and c are the parameters of the lift oscillator model to be determined around the resonance region with forced- or free-vibration tests.

Corless and Parkinson found approximate analytical solutions of Eqs. 5-7 with the method of multiple scales. The solution was then improved few years later in the primary resonance range [11]. The model was tested in the case of a two-dimensional square cylinder in an air stream with reference to the experimental results of Bearman *et al*. [12]. The agreement of numerical results with experiments was judged satisfactory, except for an overprediction of the vibration amplitude near the resonance region. In particular, the model correctly estimated the onset of the oscillations, as well as the growth of the amplitude with the wind speed outside the resonance region. For some choices of the model parameters, it also exhibited superharmonic resonance, though at a slightly higher wind speed compared to the experimental results (at $3U_r$ instead of about $2.5U_r$).

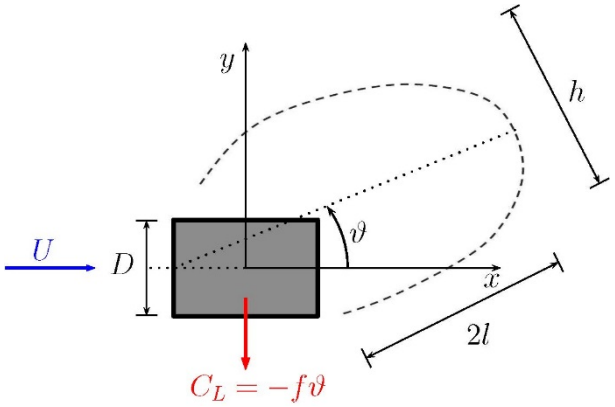

Figure 3. Schematic of the wake oscillator in Tamura and Matsui's model [13].

3.2 Tamura and Shimada's model

In 1987, Tamura and Shimada [7] proposed a similar model, once again simply summing the quasi-steady forces and the vortex-induced forces. For the latter, they adopted the model proposed by Tamura and Matsui [13] for a circular cylinder (extended to the case of a deformable slender structure in Ref. [14]) and adapted it to the case of a square cylinder. This wake oscillator model, which assumes the inclination ϑ of the wake (Figure 3) as time-dependent variable, is based on Birkhoff's oscillator model for the dead-air region behind a stationary circular cylinder [15]. Funakawa [16] had already linearly coupled Birkhoff's model with the structural oscillator, assuming that the wake oscillator is forced by the body motion (velocity and acceleration) and that the force exerted on the cylinder is proportional to the wake angle ϑ. The resulting linear coefficient f had been determined from

experimental tests on a rotating cylinder, in analogy to the Magnus effect. Nakamura [17] had considered a similar coupled linear model and treated vortex-induced vibration as binary flutter. Tamura and Matsui [13] included in the wake oscillator model the effect of fluctuation of the length of the dead-air region as a nonlinear contribution to the stiffness of the restoring spring and the effect of the discharged vortices as an equivalent negative linear damping. Finally, they obtained a Van der Pol equation for the wake angle ϑ. Once the quasi-steady forces have been added, the resulting nonlinear system of differential equations reads:

$$Y'' + 2\zeta_0 Y' + Y = -m^* V_{red}^2 f \cdot \left(\vartheta + \frac{Y'}{V_{red}} \right) + m^* V_{red}^2 \left[A_1 \frac{Y'}{V_{red}} + A_3 \left(\frac{Y'}{V_{red}} \right)^3 + \dots \right] \tag{7}$$

$$\vartheta'' - 2\beta\upsilon\vartheta' \cdot \left(1 - \frac{4f^2}{C_{L0}^2} \vartheta^2 \right) + \upsilon^2 \vartheta = -\lambda Y'' - \upsilon^2 \frac{Y'}{V_{red}} \tag{8}$$

where, after adaptation to the case of a square instead of a circular cylinder:

$$\beta = \frac{f}{2\sqrt{2}\pi^2 l^*} \qquad \lambda = \frac{1}{1+l^*} \qquad l^* = \frac{l}{D} = \frac{1}{4\pi \cdot St^2 h^*} \tag{9-11}$$

being $h^* = h/D$ the nondimensional width of the wake and f the previously mentioned coefficient of proportionality of the vortex-excited lift coefficient to the wake inclination ϑ, which can be related to the Magnus effect for a rotating cylinder [16, 17]. It is worth noting that the relations reported in Eqs. 9-11 rigorously apply for a square cylinder and should be slightly modified to account for the considered side ratio. Nevertheless, given the low sensitivity of the equation results to the value of h^*, as it will be shown in section 4.3, the equations were not modified in the analyses to follow.

Eqs. 7-8 were numerically solved for three experimental test cases of a square cylinder in an airflow. A qualitative agreement with the wind tunnel data of Wawzonek [18] was obtained, although the amplitude of oscillation was overestimated in the resonance region.

Tamura and Shimada's model presents two wake parameters, namely f and h^*, that have a clear physical meaning but can be difficult to determine. By contrast, Corless and Parkinson's model presents three empirical parameters to be calibrated through experiments (a, b and c in Eqs. 5-6). Moreover, as discussed in Ref. [11], by substituting $C'_v = -f\vartheta$ in Eqs. 7-8, one obtains a system of equations similar to those of Corless and Parkinson's model (Eqs. 5-6) but with a different phase between the unsteady transverse force C_v and the body displacement Y. The actual effect of this has not been understood yet.

4 NUMERICAL SIMULATIONS

Corless and Parkinson's and Tamura and Shimada's models were applied to the case of a rectangular cylinder with a side ratio of 1.5, for which a wide set of experimental data are available [1-3]. In particular, the measurements of vibrations of an elastically suspended plywood sectional model reported in Ref. [3] were assumed as reference for the numerical simulations. The selected test cases are shown in Figure 4 and the corresponding dynamic parameters are summarized in Table 1. In addition, the results of static tests were used to determine some of the parameters appearing in the model equations, namely the quasi-steady transverse force coefficient (Figure 5), the Strouhal number (left frame of Figure 6) and the amplitude of the fluctuating lift coefficient (right frame of Figure 6). The latter was evaluated as $C_{L0} = \sqrt{2} \cdot C_L'$, being C_L' the standard deviation of the lift coefficient time history for the stationary cylinder, bandpass filtered around the Strouhal frequency.

As shown in Figure 5, the transverse force coefficient was approximated through an 11th-order polynomial, whose coefficients are summarized in Table 2 for two values of the Reynolds number ($Re = \rho UD/\mu$, being μ the air dynamic viscosity), along with the Strouhal number and the lift coefficient amplitude for a null angle of attack. Since the slope of the polynomial approximation (coefficient A_1) is crucial to determine the quasi-steady galloping critical wind speed, it was first carefully estimated through a linear approximation in the range between -2° and +2° and it was imposed as a constraint in the least-squares fit. Polynomial approximation of any order was not able to reproduce all the features of the measured transverse force coefficient, not even with a weighted fit. For this reason, numerical simulations with the quasi-steady model using a spline interpolation of the experimental data are discussed in section 4.1. However, the 11th-order polynomial gave the best approximation of the wind tunnel results, while no significant difference in the range of angles of attack of interest was obtained with higher-order approximations. The experimental results for a lower Reynolds number were used in the numerical simulations in order to focus on the VIV-galloping interference occurring close to the resonance range (see the last column of Table 1). Nevertheless, the influence on the quasi-steady response of the variation in the transverse force coefficient due to Reynolds number was evaluated in section 4.1.

The 2nd-order differential equations of quasi-steady, Corless and Parkinson's and Tamura and Shimada's models were numerically solved by means of *ODE45* Matlab® function, employing the explicit Runge-Kutta method and specifically the Dormand-Prince algorithm that uses six function evaluations to calculate fourth- and fifth-order accurate solutions. Some control parameters, such as relative and absolute tolerances, have been properly tuned beforehand, so to optimize the accuracy of the solution. It is also worth noting that, prior to starting the numerical analyses of sections 4.2 and 4.3, the numerical codes to solve the systems of differential equations were verified on the case of a square cylinder, for which old numerical solutions are available (see Ref. [19]).

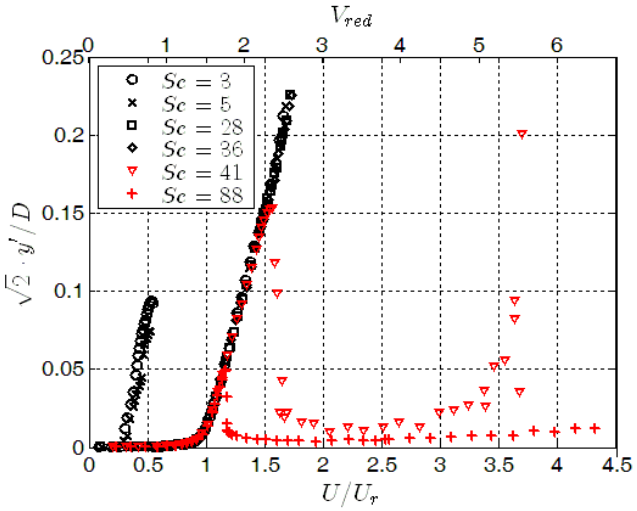

Figure 4. Nondimensional amplitude of vibration of the rectangular cylinder measured in the wind tunnel for various flow speeds and different values of the Scruton number [3].

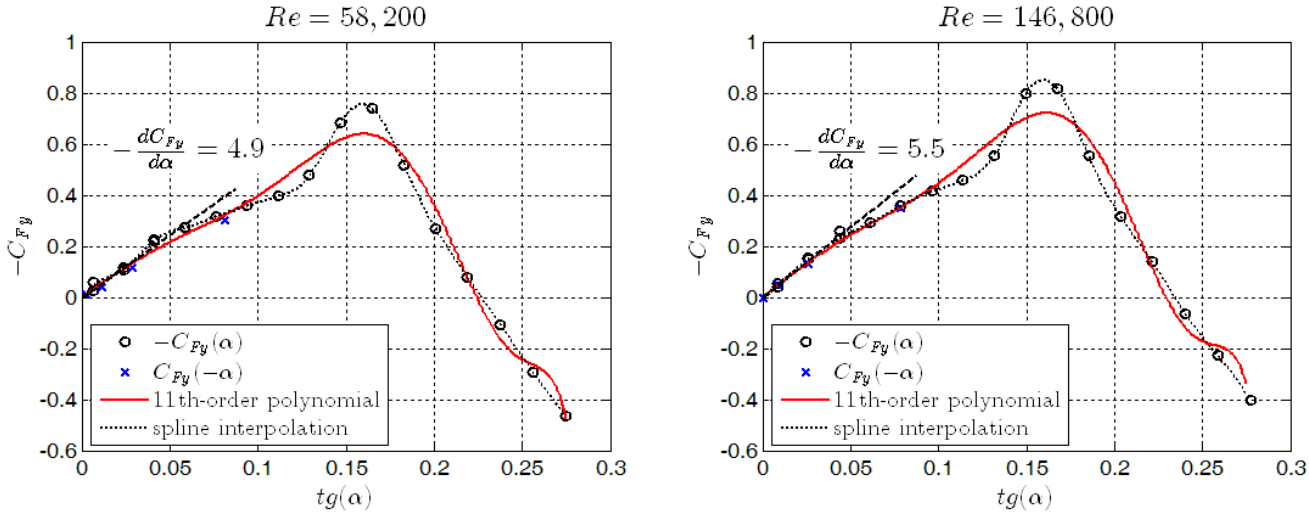

Figure 5. 11th-order polynomial approximation of the transverse quasi-steady force coefficient (Eqs. 1-2) measured in the wind tunnel for two values of the Reynolds number. The slope of the polynomial in the origin is highlighted in the figures.

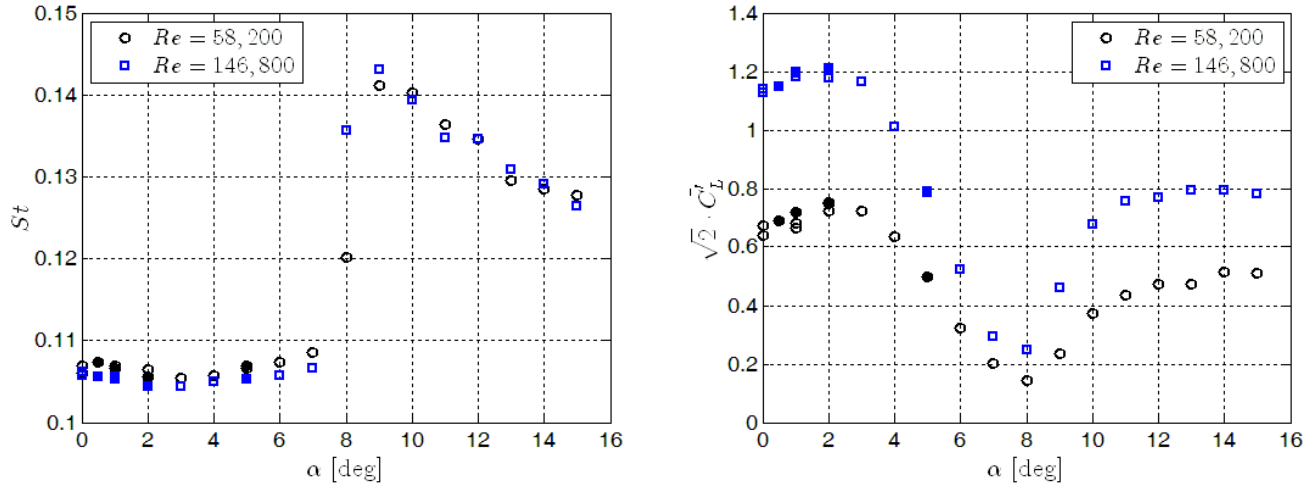

Figure 6. Strouhal number (left) and sinusoidal-equivalent amplitude of the fluctuating lift coefficient produced by vortex shedding (right) measured in the wind tunnel for various angles of attack at two different Reynolds numbers.

Table 1. Experimental case studies considered for the numerical simulations. M is the effective mass of the oscillating system, $m^* = \rho D^2 L/M$ and $Sc = 4\pi M\zeta_0/\rho BDL$ are respectively the mass ratio and the Scruton number, being D = 77 mm and B = 116 mm the cross-wind and streamwise section dimensions and L = 986 mm the length of the model; $U_g = 2Sc/A_1 \cdot n_0 B$ is the quasi-steady galloping critical wind speed, calculated for A_1 = 4.88 (see Table 2); $Re_r = \rho U_r D/\mu$ is the Reynolds number corresponding to the vortex-resonance wind speed U_r.

#	n_0 [Hz]	ρ [kg/m^3]	M [kg]	ζ_0 [%]	m^* [-]	Sc [-]	U_g/U_r [-]	Re_r [-]
1	9.04	1.21	5.526	0.045	6.4e-04	2.9	0.19	33,700
2	9.26	1.20	5.228	0.084	6.7e-04	5.1	0.34	34,500
3	9.06	1.22	5.526	0.44	6.5e-04	28.0	1.86	33,800
4	9.02	1.22	5.526	0.57	6.5e-04	36.2	2.40	33,600
5	9.02	1.21	5.526	0.64	6.4e-04	41.4	2.75	33,600
6	9.01	1.20	5.526	1.35	6.3e-04	87.7	5.82	33,600

Table 2. Coefficients of the 11th-order polynomial approximation of the transverse force coefficient measured in the wind tunnel for two Reynolds numbers. The values of the Strouhal number and of the sinusoidal-equivalent amplitude of the fluctuating lift coefficient produced by vortex shedding are also reported.

Re [-]	A_1 [-]	A_3 [-]	A_5 [-]	A_7 [-]	A_9 [-]	A_{11} [-]	St [-]	C_{L0} [-]
58,200	4.88	-2.909e02	3.014e04	-1.173e06	1.733e07	-8.749e07	0.106	0.656
146,800	5.50	-3.182e02	3.215e04	-1.231e06	1.798e07	-8.977e07	0.106	1.133

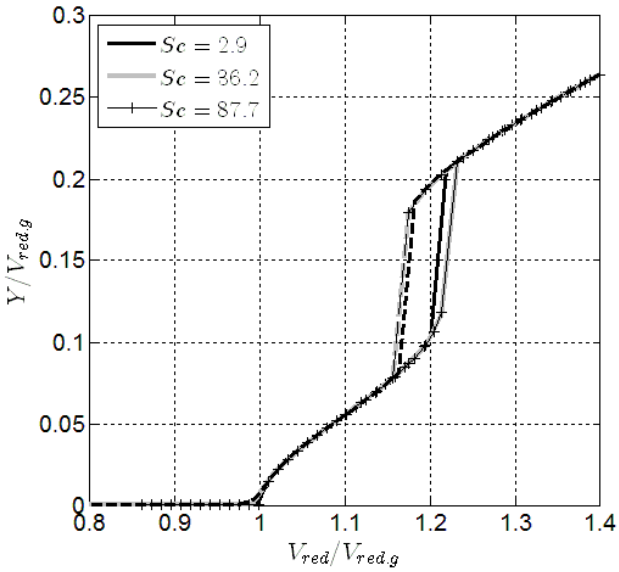

Figure 7. Universal plot of the amplitude-velocity curves obtained with the quasi-steady model for different values of the Scruton number (cases #1, #4 and #6 of Table 2). Solid and dashed lines indicate respectively solutions obtained from initial conditions $Y(0) = 0.01$, $Y'(0) = 0$ and from $Y(0) = 15° \cdot \pi/180 \cdot V_{red}$, $Y'(0) = 0$. $V_{red,g} = U_g/2\pi n_0 D$ is the galloping critical reduced wind speed.

4.1 Quasi-steady model results

Prior to undertaking the analysis of numerical models of interference between VIV and galloping, the response of the considered rectangular 3:2 cylinder was calculated with the quasi-steady model (Eq. 4). Simulations were carried out for the test cases reported in Table 1, calculating the amplitude-velocity curves with the polynomial approximation of the transverse force coefficient measured for low Reynolds number (first row of Table 2). Two different initial conditions were considered, namely a small initial amplitude ($Y(0) = 0.01$) and null velocity ($Y'(0) = 0$) and a higher value of $Y(0)$, compatible with the maximum angle for which the transverse force coefficient was measured in the wind tunnel (Figure 5), and null velocity. Figure 7 reports the results for three different test cases in the collapsed form adopted in Ref. [9]. It is apparent that the different curves only differ in the hysteresis loop, which is slightly smaller for lower values of the Scruton number. It is worth noting that the 11th-order polynomial approximation of the transverse force coefficient produces a galloping response qualitatively with the same features as a 7th-order polynomial (see *e.g.* Ref. [20]).

It is clear from Figure 5 that the 11th-order polynomial approximation is not able to follow the actual features of the measured transverse force coefficient, in particular in the region of the pronounced peak. To shed some light on the effects of this, a spline-based numerical approach was used to estimate the amplitude-velocity response curves. First, the C_{Fy} function was defined by using a spline that interpolates the experimental data points (Figure 5). Second, a numerical integration scheme based on the 2nd-order finite difference method was adopted, in which at each time step the fluid force is calculated according to the previously mentioned spline interpolation of the wind tunnel data.

Figure 8 compares the C_{Fy} polynomial functions for two Reynolds numbers with the corresponding splines. It is apparent that, for both Reynolds numbers, the spline interpolation provides a more irregular pattern than the corresponding polynomial function with a more pronounced peak. Figure 9 compares the non-dimensional responses obtained by considering a polynomial fit and a spline interpolation of the measured C_{Fy} for the lower Reynolds number. The results confirm the expected influence of the actual measured pattern of C_{Fy} on the response. First, in the "spline case", the oscillation starts at a reduced velocity lower than that predicted by using the polynomial function. As shown in Figure 8, this behavior derives from the higher slope of the spline very close to the origin, giving rise to a lower value of the galloping critical wind speed. Nevertheless, after the oscillation onset, the growth rate with the reduced velocity is small since the spline shows an inflection point for a very small angle of attack. It is not clear if this behavior is physical or simply due to small measurement errors in the C_{Fy} values near the origin (Figure 5), as pure quasi-steady galloping was not observed in the experiments [3]. Nevertheless, the analysis discussed here clarifies the importance of small differences in the considered pattern of the transverse force coefficient, especially in the neighborhood of a null angle of attack.

In Figure 9, one can also observe the presence of two hysteresis loops in the spline case and just one in the polynomial case. In addition, the extension of the second hysteresis loop is larger for the spline interpolation. Barrero-Gil *et al.* [20] showed that the inflection points in the transverse force coefficient pattern correspond to the saddle points in the response plot. For the apparent angles of attack attained, the 11th-order polynomial approximation of C_{Fy} shows two saddle points, which correspond to a single hysteresis loop in the response plot (Figure 8 and Figure 9). By contrast, as shown in Figure 10, the spline function shows more inflection points in the range of apparent flow incidences reached during the oscillations. Nevertheless, just two pairs of them correspond to hysteresis loops in the amplitude-velocity curve. It is also worth noting that the responses in the upper branch predicted in the two cases are nearly the same. This is due to the similar pattern of the descendent branch of C_{Fy} in case of polynomial approximation and spline interpolation of the experimental data. Nevertheless, Figure 11 clearly shows that the transient to reach the same steady-state amplitude is very different in the two cases. In fact, the build-up is faster in the spline case, due to the higher C_{Fy} peak, and the time-history envelop presents two inflection points instead of one.

The effect on the quasi-steady galloping behavior of the difference between the transverse force coefficients measured for two different Reynolds numbers was also investigated (Figure 5 and Figure 8). Figure 12 reports the response obtained by interpolating the C_{Fy} with splines in the two cases. It can be seen that the response is quite different in all the reduced velocity ranges. In addition, the amplitude-velocity curve presents a single hysteresis loop for the higher Reynolds number. The larger response for high reduced wind speed is due to the larger angle of attack for which C_{Fy} changes sign for the higher Reynolds number.

The important role played by the approximation of the experimental values of the quasi-steady transverse force coefficient is clear. Nonetheless, in the numerical simulations to follow, only the 11th-order polynomial approximation for the lower Reynolds number value was used, as the main focus of the analysis was on the qualitative behavior of Corless and Parkinson's and Tamura and Shimada's models for VIV-galloping interference and the polynomial functions for C_{Fy} allowed much faster calculations.

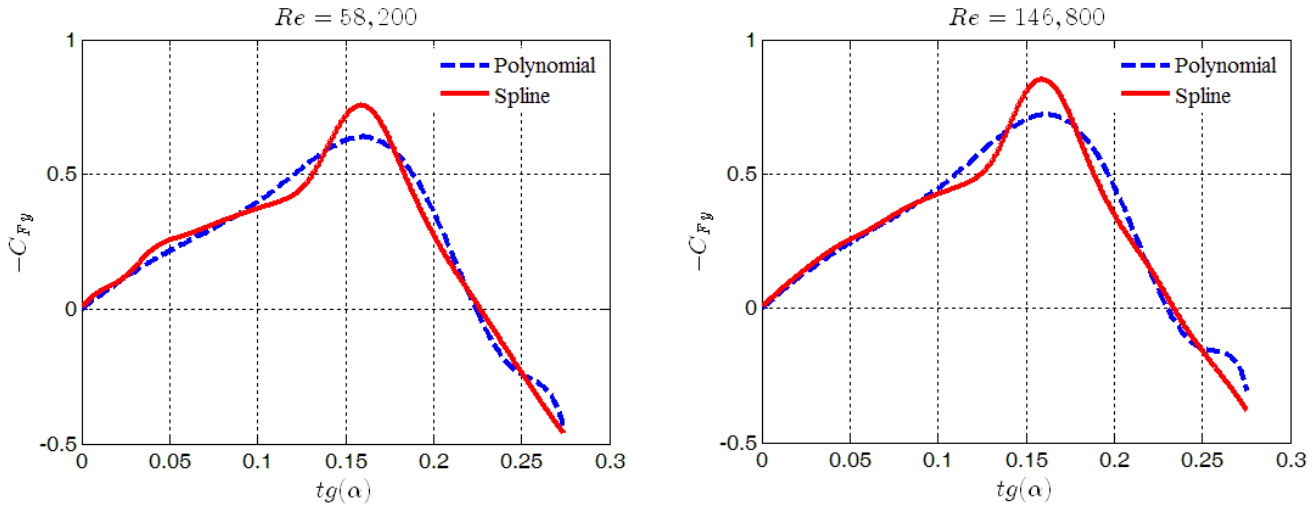

Figure 8. Comparison between the transverse force coefficient C_{Fy} fitted by a 11th-order polynomial function (dashed lines) and its interpolation with a spline (solid lines) for a Reynolds number of 58,200 (left) and 146,800 (right).

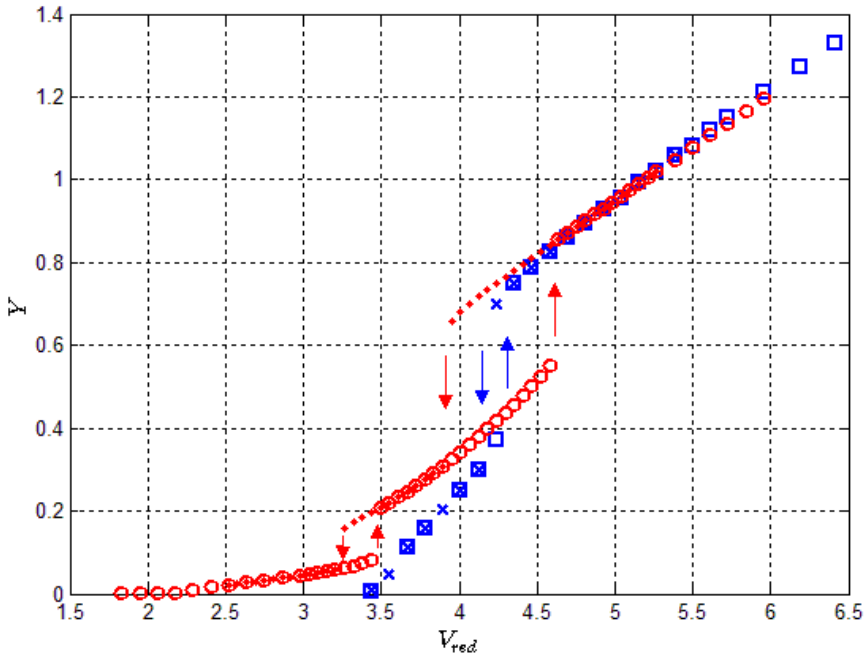

Figure 9. Quasi-steady non-dimensional transverse response against the reduced flow velocity using a transverse force coefficient C_{Fy} approximated by a 11th-order polynomial function (square and cross markers) and interpolated by a spline function (empty and circles and dots). Empty Circles and squares indicate solutions obtained from initial conditions $Y(0) = 0.01$, $Y'(0) = 0$, while dots and crosses from $Y(0) = 15° \cdot \pi/180 \cdot V_{red}$, $Y'(0) = 0$.

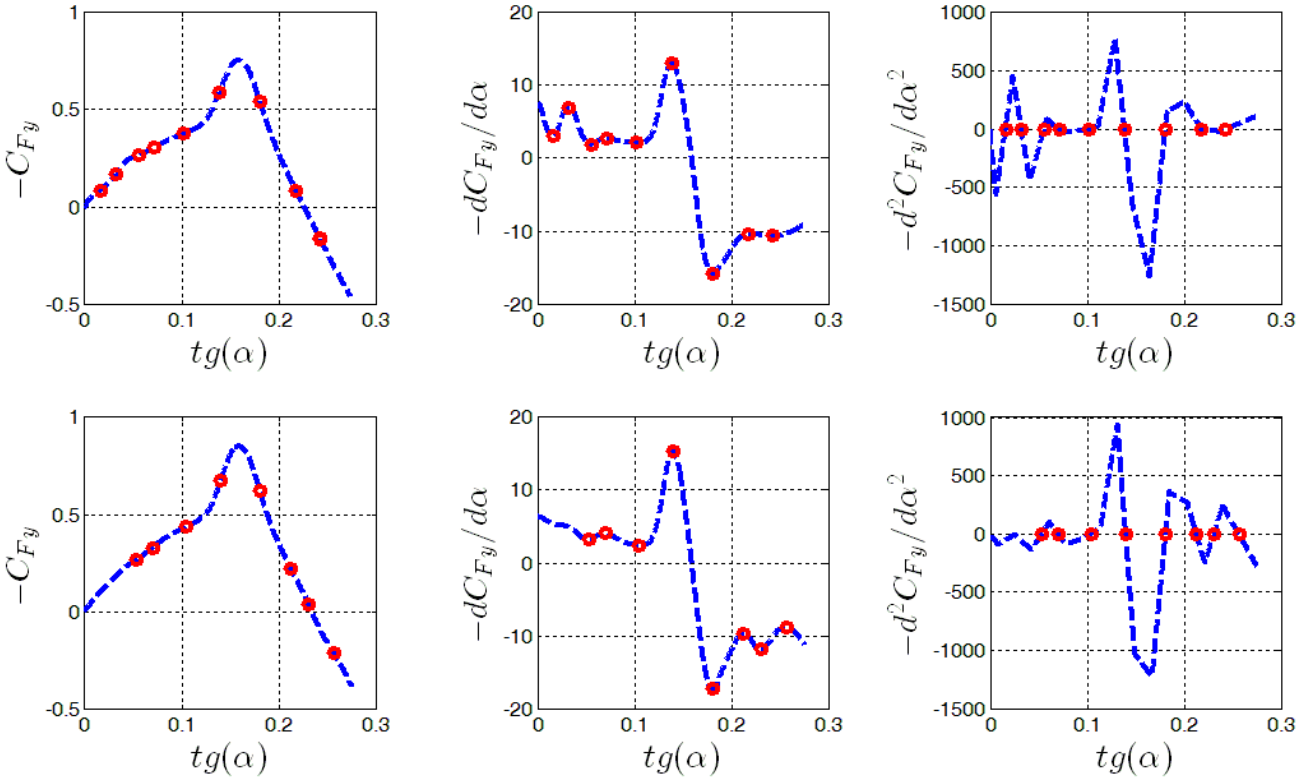

Figure 10. Spline functions interpolating the transverse force coefficient C_{Fy} and its first two derivatives for a Reynolds number of 58,200 (top) and 146,800 (bottom); inflection points are highlighted (red circles).

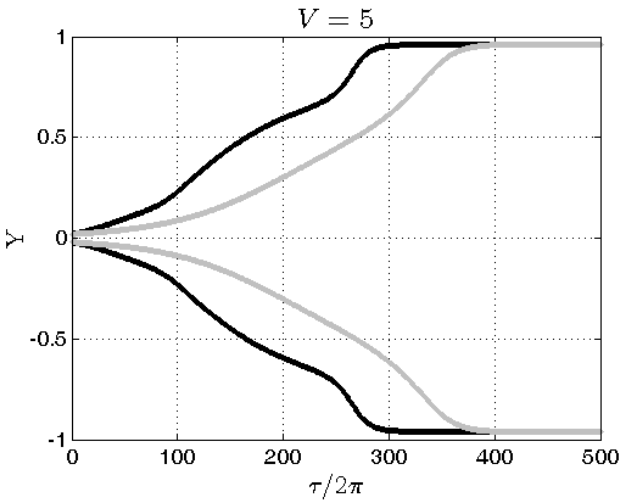

Figure 11. Comparison of the build-up time-history envelop from $Y(0) = 0.01$, $Y'(0) = 0.01$ in case of spline interpolation (black line) and 11th-order polynomial approximation (grey line) of the experimental transverse force coefficient C_{Fy} (Re = 58,200).

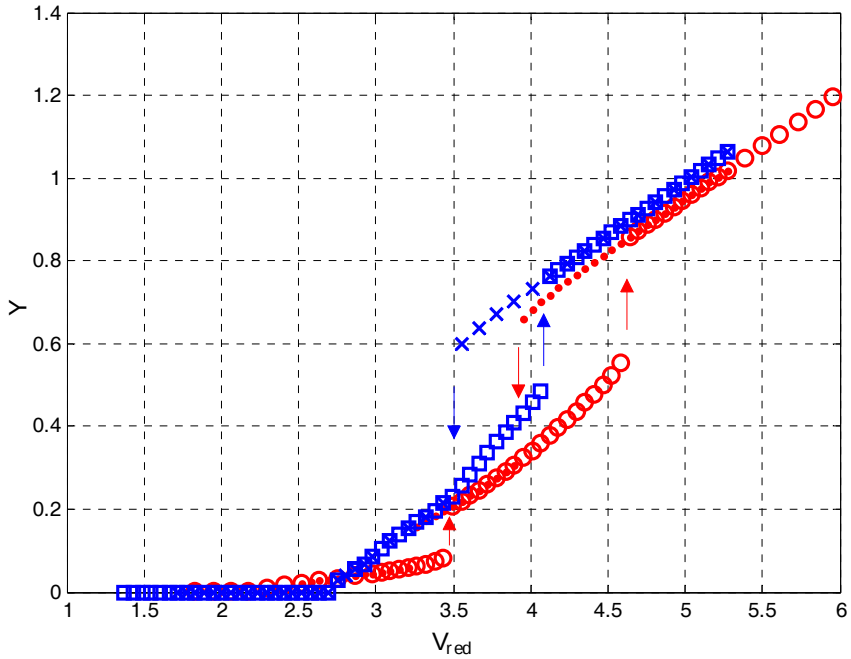

Figure 12. Quasi-steady non-dimensional transverse response against the reduced flow velocity using a spline interpolation of C_{Fy}: Re = 58,200 (empty circles and dots) and Re = 146,800 (square and cross markers). Empty Circles and squares indicate solutions obtained from initial conditions $Y(0) = 0.01$, $Y'(0) = 0$, while dots and crosses from $Y(0) = 15° \cdot \pi/180 \cdot V_{red}$, $Y'(0) = 0$.

4.2 Corless and Parkinson's model results

As previously mentioned, the procedure to identify the parameters a, b, c appearing in Hartlen and Currie's model, integrated in Corless and Parkinson's model (see Eq. 6), would require either forced-vibration tests or a vortex-induced response optimization procedure. In the latter case, a condition showing remarkable self-excited effects should be considered to enable a correct identification of the parameters. This means that the results obtained for a low value of the Scruton number are expected to be used. Nevertheless, in the case of the rectangular 3:2 cylinder this is not possible since VIV and galloping strongly interact in case of low mechanical dissipation capability of the system. For this reason, the analysis was carried out by considering as nominal values of the parameters those determined by Hatlen and Currie with forced-vibration tests for a square cylinder reported in Table 3 (see also Ref. [10]) and performing a wide sensitivity study on the effects of each single model parameter.

Given the low Reynolds number at which the VIV-galloping instability onset in the dynamic tests in the wind tunnel [3] (see also the last column of Table 1), the value $C_{L0} = 0.656$ determined for a value of the Reynolds number equal to 58,200 was assumed in the numerical simulations. However, in view of the great variability and uncertainty of this parameter, a sensitivity analysis was carried out also in this case.

Table 3. Nominal values of the unsteady parameters set in Corless and Parkinson's model.

a	b	c	St	C_{L0}
0.13	-2.35	0.855	0.106	0.656

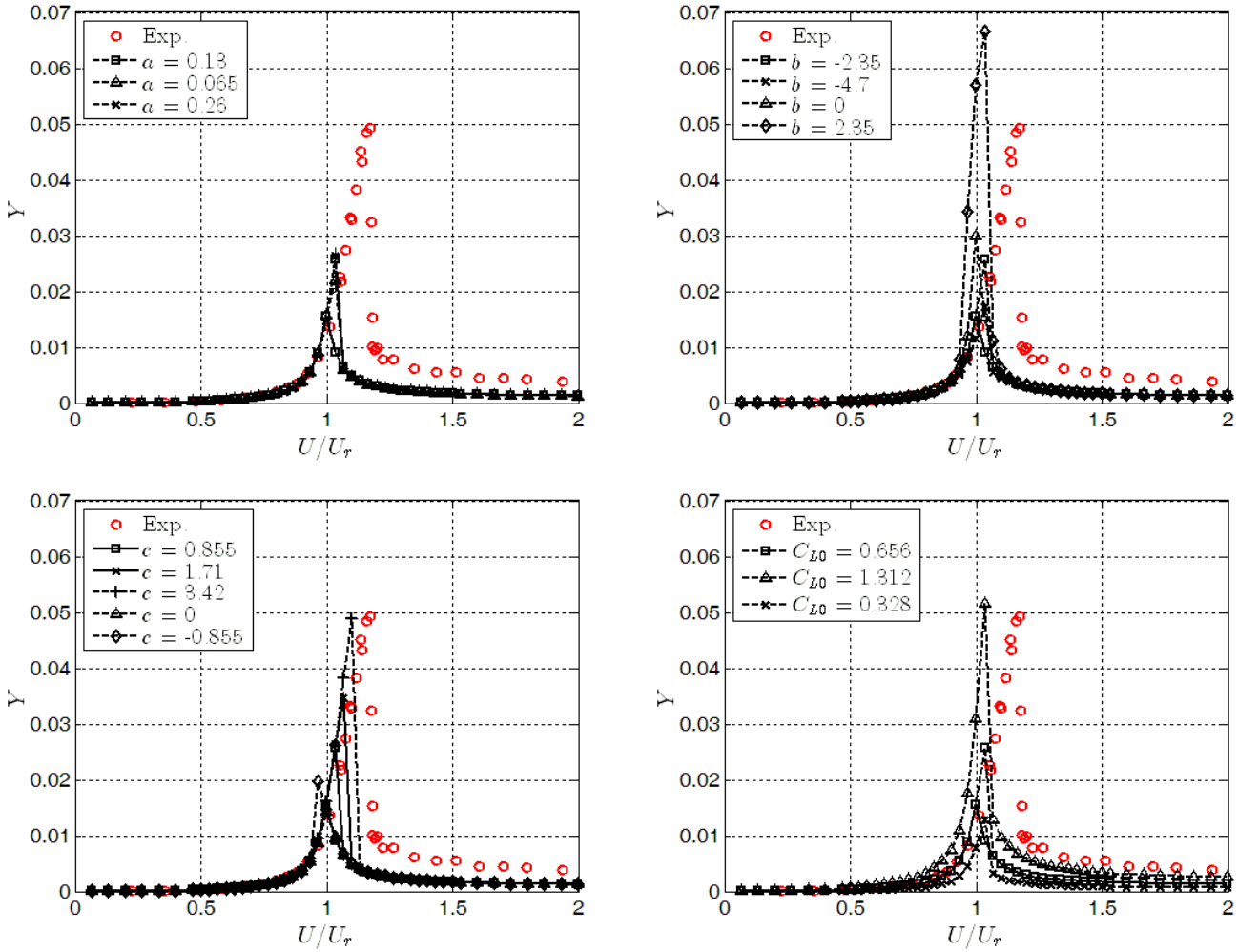

Figure 13. Comparison between experimental and numerical results obtained with Corless and Parkinson's model for Sc = 87.7 (test case #6). Solid and dashed lines indicate respectively solutions obtained from initial conditions $Y(0)$ = 0.01, $Y'(0)$ = 0 and from $Y(0) = 15° \cdot \pi/180 \cdot V_{red}$, $Y'(0)$ = 0.

For strictly positive parameters (a and C_{L0}), half and double values were considered in the sensitivity study along with the nominal values. By contrast, for the other parameters (b and c) the nominal values were doubled, zeroed and changed of sign. In particular, for the parameter c, which plays a critical role in the interference between VIV and galloping, also simulations with four times its nominal value were performed.

The investigation started with a test case (#6 in Table 1) wherein no VIV-galloping interference occurred, in order to understand which values of the parameters allow to better reproduce the VIV response of the system. However, as previously said, the high value of the Scruton number (Sc = 87.7) only enables to obtain indicative and qualitative information from this preliminary study about the correct model parameters. Figure 13 clearly shows that with the assumed nominal values of the parameters the VIV peak amplitude is significantly underestimated. The rate of increase of the limit-cycle amplitudes is slightly higher and the resonance curve is even narrower than in the experiments. It is also noteworthy that, as expected, the numerical results exhibit a small hysteresis loop. The doubling of the value of the parameter a entails only a small reduction of the response peak amplitude, while by halving it one obtains a slightly larger reduction of the response but still not much significant. Consequently, it is possible to conclude that for such a high Scruton number the VIV prediction of Hartlen and Currie's model is not very sensitive to large variations of the parameter a around the nominal value estimated for the square cylinder. By contrast, the value of b in Eq. (4) significantly influences the results of the numerical calculations. In particular, the limit-cycle oscillation amplitudes remarkably increase if b takes positive values, while the influence on the results is small if the negative nominal value of the parameter is either doubled or halved. Nevertheless, by setting a positive value of b the peak of the response curve shifts towards lower values of the wind speed, in disagreement with experiments. Conversely, critical seems to be the role played by the parameter c: in fact,

if this is increased as compared to the assumed nominal value, the peak amplitude increases and its position shifts towards higher wind speeds, in agreement with experiments. The wind tunnel data are satisfactorily matched for c = 3.42, *i.e.* four times the nominal value 0.855. A double value of C_{L0} (close to the value measured for high Reynolds number, as shown in Table 2) produces a peak response close to the experimental value, but in this case the corresponding wind speed is appreciably lower. Finally, it is worth noting that whatever values of the parameters tested do not significantly influence the width of the calculated response curve, which remains roughly as narrow as it is in the experiments.

After this preliminary investigation, test case #1 in Table 1 was studied. It is characterized by a low Scruton number and consequently by a theoretical quasi-steady galloping critical wind speed much lower than the vortex-resonance wind speed. The results of the numerical calculations are shown and compared with experiments in Figure 14. Considering the simulations with the nominal values of the model parameters, it is to note that the model predicts a self-limited response at reduced wind speeds lower than the vortex-resonance velocity, where the main velocity-unrestricted instability starts. The calculated amplitudes for $U/U_r > 1$ are significantly higher than those observed in the wind tunnel and do not follow a nearly linear trend as the latter. However, the developed galloping branch for $U/U_r > 1.5$, which asymptotically tends to the quasi-steady prediction, shows the same slope as the experimental data. The model parameter a has practically no effect on the response curve beyond the vortex-resonance wind speed. A significant increase of it just contributes to reduce the range of the secondary instability at low reduced wind speed. By contrast, to double the reference value of b allows to slightly reduce the slope of the response curve in the range $1 < U/U_r < 1.5$ but this continues to be much higher than in the experiments. Another effect is the reduction of the amplitudes of the secondary excitation predicted at low reduced wind speed. The opposite behavior is observed if b is either reduced in magnitude or set to a positive value. The variation of the parameter c plays a role also in the response curve beyond $U/U_r \approx 1.5$, with the different curves slowly converging to the quasi-steady limit. It is also worth noting that no secondary excitation is predicted for values of c equal to two or four times the assumed nominal value 0.855. By contrast, a null or negative value of c enhances the response at low reduced wind speed and slightly delays the onset of the main instability. The bottom right frame of Figure 14 shows that a significant variation of the value of C_{L0} has an effect on the low reduced wind speed self-limited instability and in the range $1 < U/U_r < 1.5$: in both cases, the oscillation amplitudes increases if C_{L0} is set to a larger value.

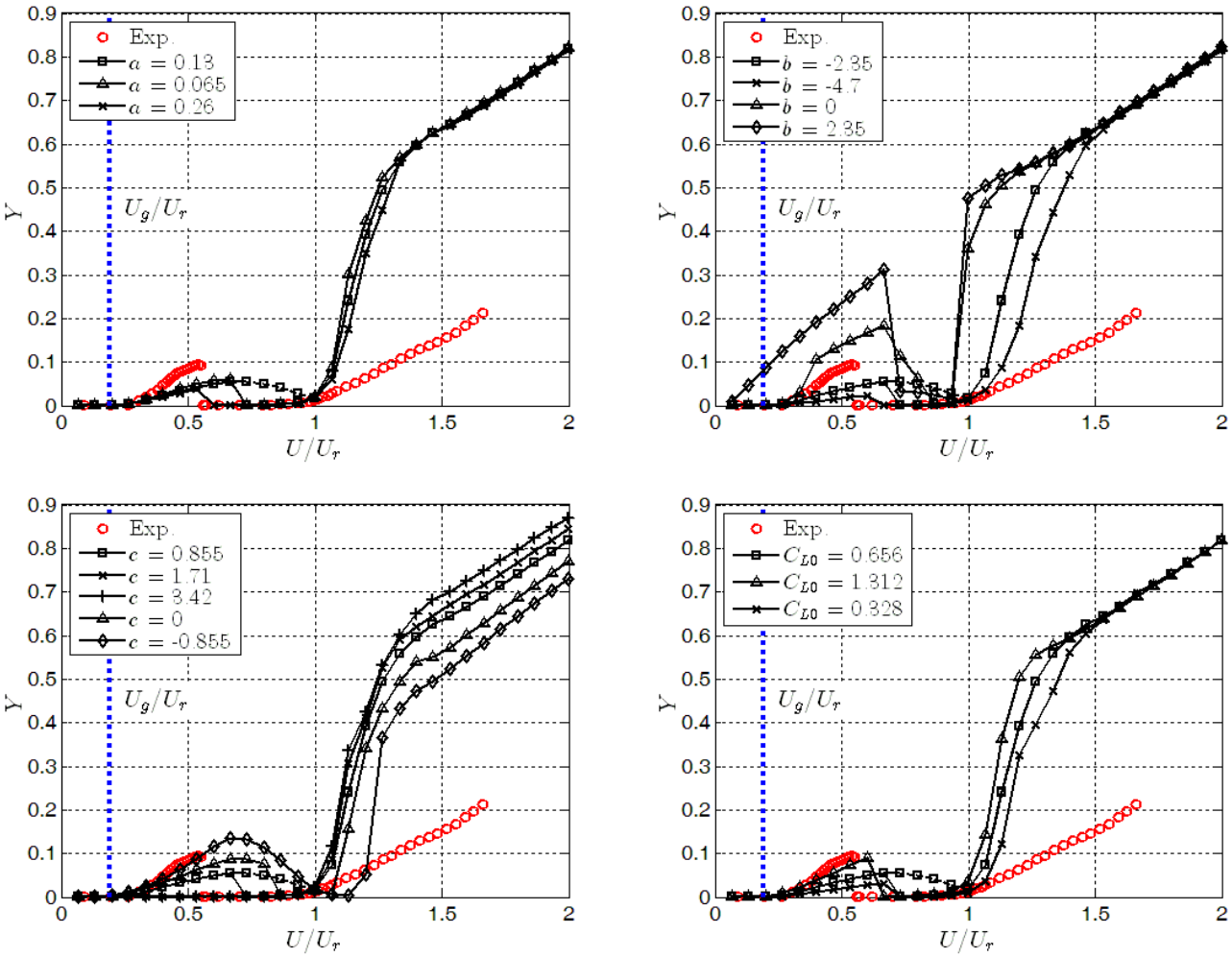

Figure 14. Comparison between experimental and numerical results obtained with Corless and Parkinson's model for Sc = 2.9 (test case #1). Solid and dashed lines indicate respectively solutions obtained from initial conditions $Y(0) = 0.01$, $Y'(0) = 0$ and from $Y(0) = 17° \cdot \pi/180 \cdot V_{red}$, $Y'(0) = 0$.

A secondary excitation was also observed in the experiments for low values of the Scruton number and it was interpreted as a third-order superharmonic resonance [1-3]. Despite the fact that the theoretical quasi-steady galloping critical wind speed falls in the neighborhood of the onset of the oscillations, the strong dependence on the value of C_{L0} corroborates the conjecture that this is a secondary resonance excitation. In order to further investigate this issue, the low reduced wind speed response was calculated for two slightly higher values of the Scruton number. The results are reported in Figure 15. Unlike the experiments, the onset of the secondary instability is delayed when the system damping is increased but it does not coincide with the quasi-steady galloping critical flow speed.

Figure 16 clarifies that the unsteady force due to vortex shedding C_v is synchronized with the body motion in the range $1 < U/U_r < 1.5$. Then, around $U/U_r = 1.5$ desynchronization occurs, so that the force C_v starts to oscillate again at the vortex-shedding frequency and the response converges to the quasi-steady limit. It is worth remarking that in the experiments, up to a certain Scruton number, the system response changes from quasi-periodic to periodic around $U/U_r = 1.5$ [1-3], while for Sc larger than about 40, when VIV and galloping instabilities first separate (see Figure 4 and Ref. [3]), the oscillations cease just at $U/U_r \approx 1.5$.

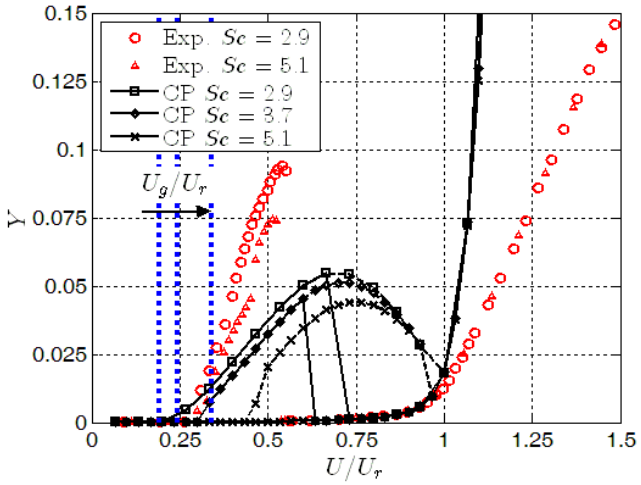

Figure 15. Comparison between experimental and numerical results obtained with Corless and Parkinson's model (CP) for three different Scruton numbers. Solutions were obtained from initial conditions $Y(0) = 17° \cdot \pi/180 \cdot V_{red}$, $Y'(0) = 0$, using the nominal values of the model parameters.

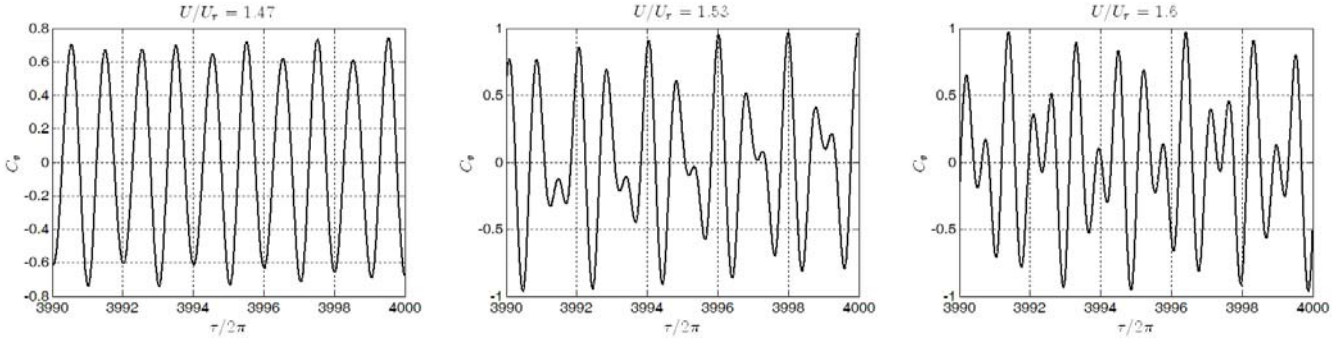

Figure 16. Time history of the force coefficient related to vortex shedding for $Sc = 2.9$ (test case #1) and nominal values of the model parameters at the beginning of the desynchronization. $\tau/2\pi$ corresponds to the number of oscillation cycles at the oscillator natural frequency n_0.

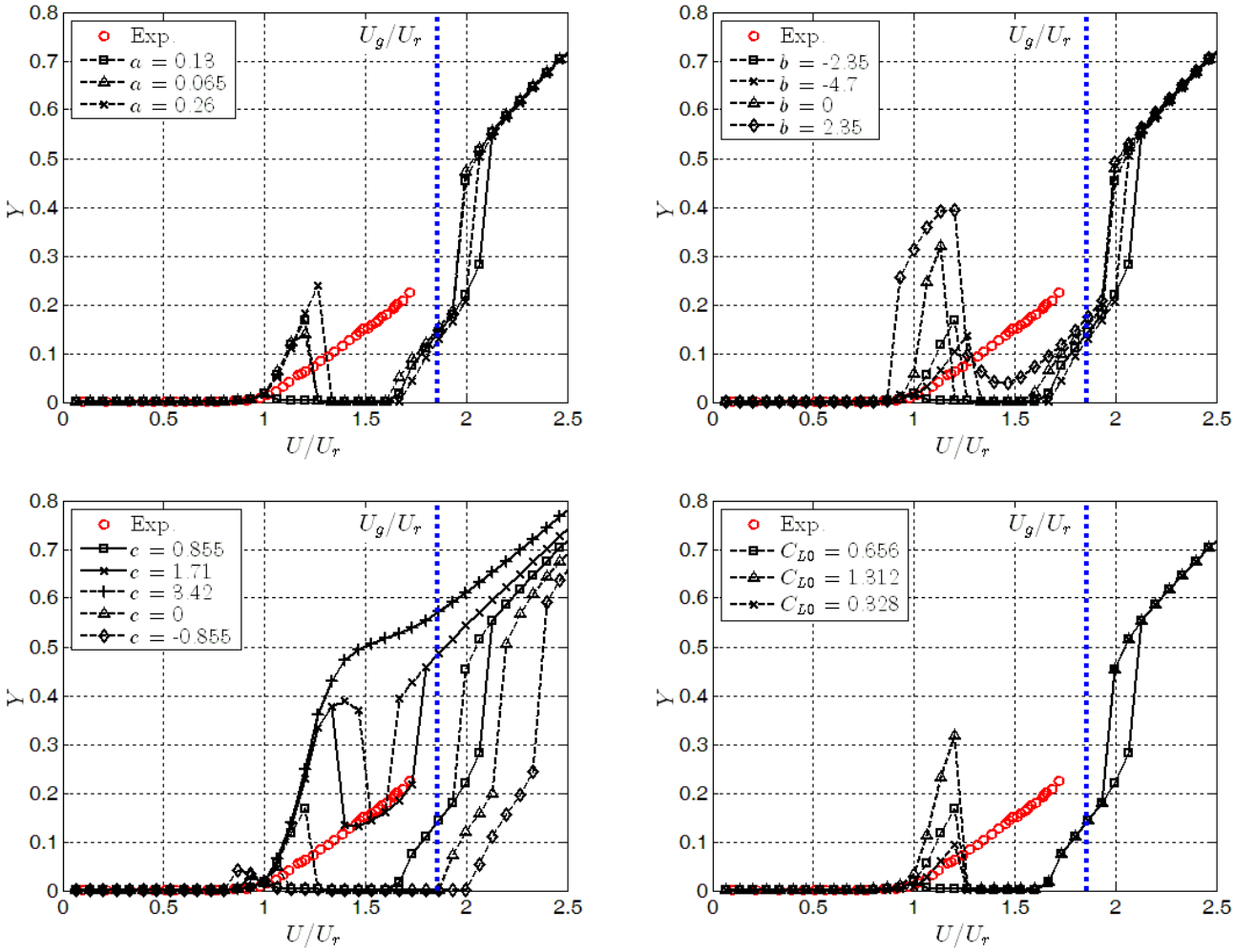

Figure 17. Comparison between experimental and numerical results obtained with Corless and Parkinson's model for Sc = 28.0 (test case #3). Solid and dashed lines indicate respectively solutions obtained from initial conditions $Y(0) = 0.01$, $Y'(0) = 0$ and from $Y(0) = 15° \cdot \pi/180 \cdot V_{red}$, $Y'(0) = 0$.

The following test case considered (test case #3 in Table 1) refers to a Scruton number of 28.0, that is a ratio $U_g/U_r = 1.86$. It is apparent in Figure 17 that the calculation with the nominal values of the model parameters predicts a full separation between the range of VIV and galloping excitation, although the galloping critical wind speed is slightly lower than that predicted by the quasi-steady theory. The galloping critical threshold and response curve coincides with the quasi-steady prediction if $c = 0$, while the instability is significantly postponed if $c < 0$. By contrast, if c is set to 1.71 (double than the nominal value), the amplitude-velocity curve calculated with Corless and Parkinson's model does not fall to zero after the peak of the VIV response but jumps down to a branch close to the linear pattern followed in the experiments. Then, in the neighborhood of the quasi-steady galloping critical wind speed, the numerical response curve shows a discontinuity, jumping up to a linear branch progressively approaching the quasi-steady result for high reduced wind speeds. If c is set to 3.42 (four times the nominal value of the parameter), even a stronger interference between VIV and galloping is obtained, with a response pattern similar to that predicted in the case of very low Scruton number (Figure 14). Figure 17 also shows that the model parameters a, b and above all C_{L0} mainly influence the VIV excitation range, although a small VIV-galloping interaction is obtained if b is set to a positive value equal in magnitude to the nominal value.

For the highest value of the Scruton number for which full VIV-galloping interaction was observed in the experiments (Sc = 36.2, test case #4 in Table 1), no significant interference was predicted by Corless and Parkinson's model (Figure 18). The only exception is the result for $c = 3.42$ (four times the nominal value), which follows a pattern very similar to that obtained in the previous test case for $c = 1.71$ (Figure 17). A similar behavior was retrieved for test case #5 (Sc = 41.4, the lowest Scruton number for which the experiments exhibited separate VIV and galloping excitations) but in this case, even for the largest value considered of the parameter c (c = 3.42), separated VIV and galloping responses were calculated (Figure 19). Nonetheless, it is to note that an increase of the value of the parameter c entails a reduction of the galloping critical wind speed. In addition, if a positive value of b is set in the model equations, the VIV response of the system is strongly enhanced.

Finally, Figure 20 shows the time histories of the limit-cycle oscillations corresponding to a few particular reduced wind speeds for test case #3 (Sc = 28.0). For a flow speed equal to one-third of the vortex-resonance velocity, one can observe a very small

excitation. At $U = U_r$ and in all the VIV excitation range, the response of the system is perfectly harmonic, while very small amplitude modulations can be detected immediately after the galloping onset ($U/U_r = 1.67$) but they quickly disappear as the wind speed is increased. For a flow speed equal to twice or three times the vortex-resonance wind velocity, sub-harmonic resonances occur and small but appreciable modulations appear in the response. The same behavior was observed in all the test cases considered but it is different from the response features shown in the wind tunnel. In fact, significant amplitude modulations occurred in the experimental VIV-galloping response for U/U_r in the range 1 – 1.5 [1-3], as typical of quasi-periodic galloping [21-23].

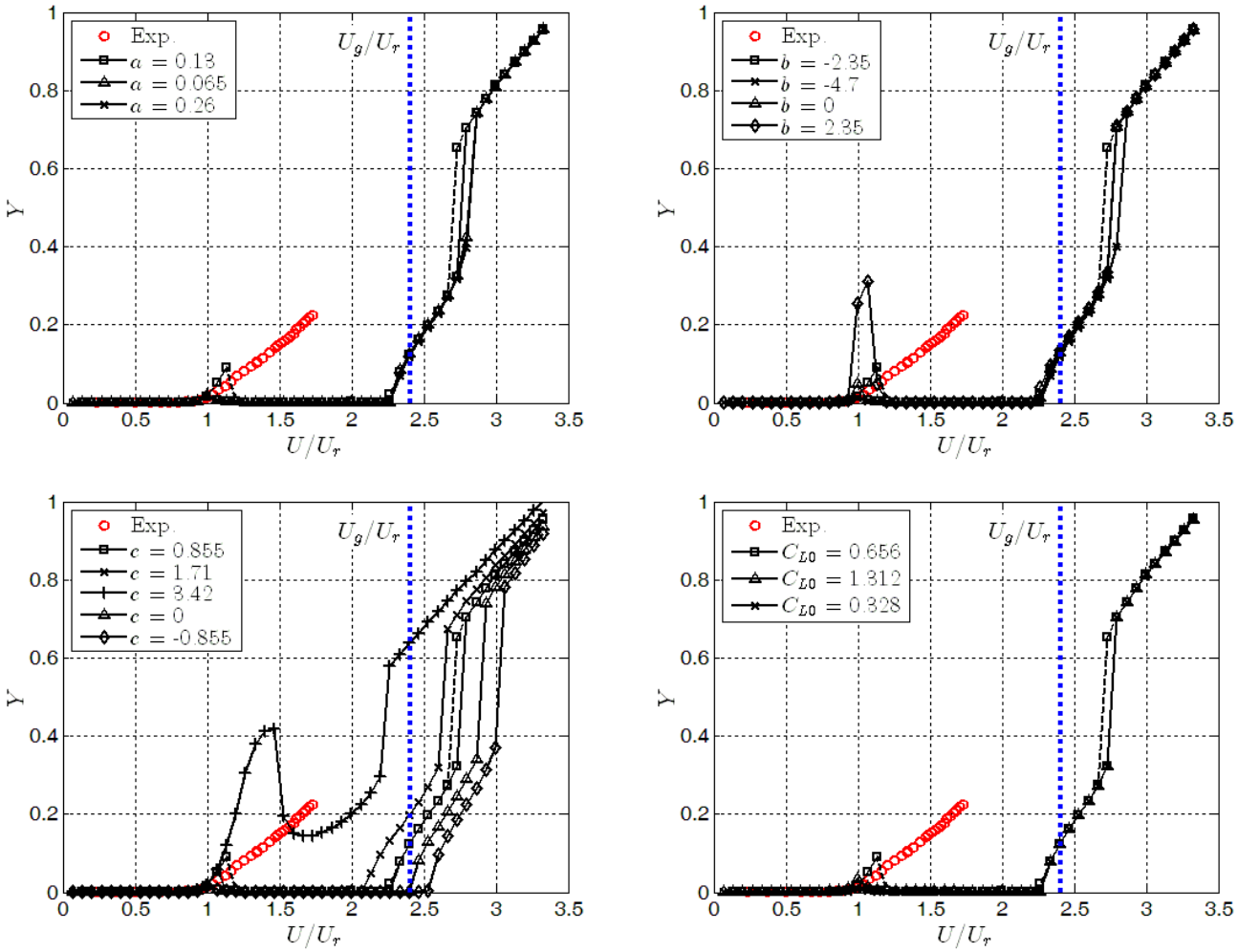

Figure 18. Comparison between experimental and numerical results obtained with Corless and Parkinson's model for $Sc = 36.2$ (test case #4). Solid and dashed lines indicate respectively solutions obtained from initial conditions $Y(0) = 0.01$, $Y'(0) = 0$ and from $Y(0) = 15° \cdot \pi/180 \cdot V_{red}$, $Y'(0) = 0$.

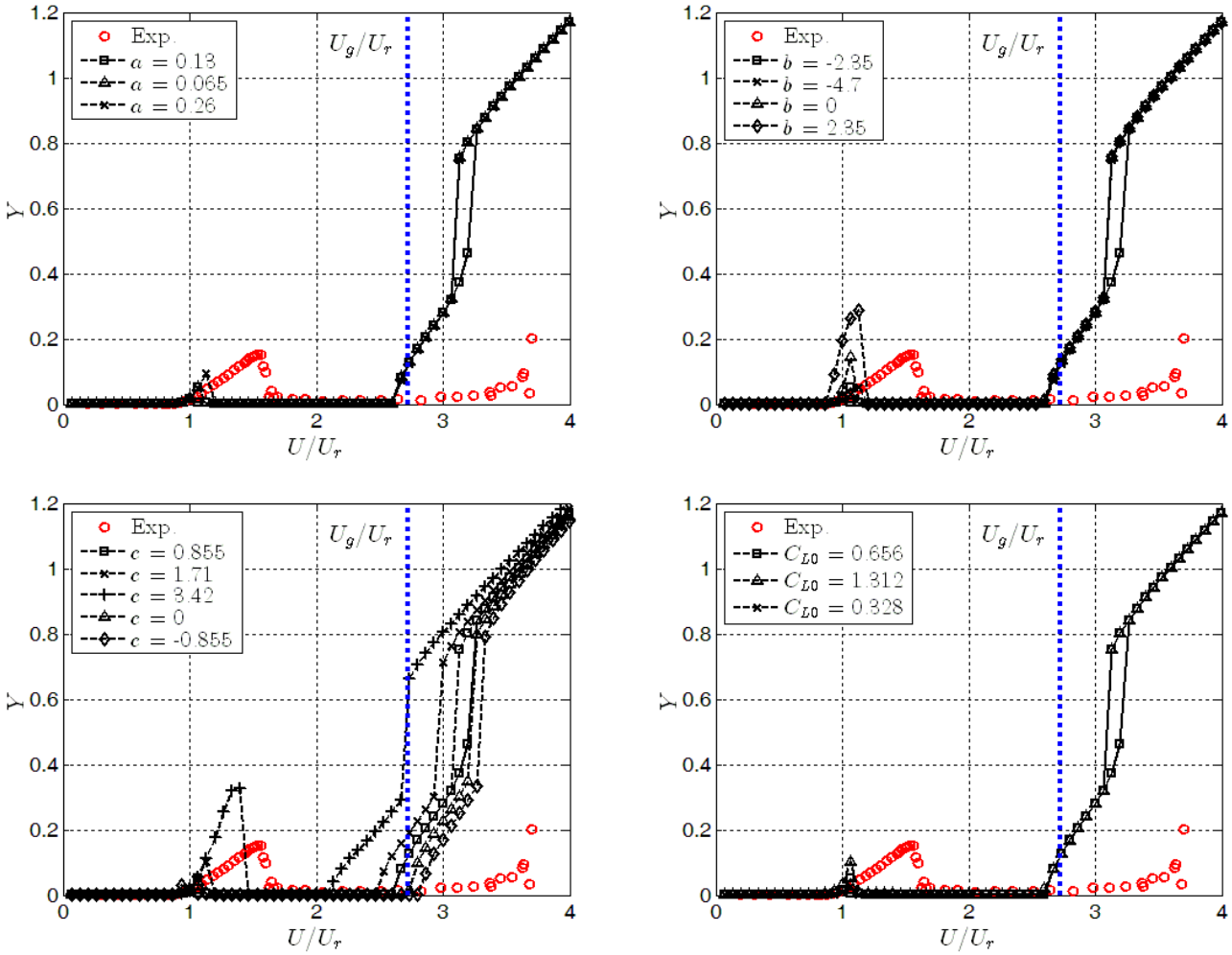

Figure 19. Comparison between experimental and numerical results obtained with Corless and Parkinson's model for Sc = 41.4 (test case #5). Solid and dashed lines indicate respectively solutions obtained from initial conditions $Y(0) = 0.01$, $Y'(0) = 0$ and from $Y(0) = 15° \cdot \pi/180 \cdot V_{red}$, $Y'(0) = 0$.

4.3 Tamura and Shimada's model results

A similar analysis to that just proposed for Corless and Parkinson's model was also performed for Tamura and Shimada's model. The same reference values of the parameters f and h^* proposed in Ref. [7] were adopted (Table 4). Those data were originally derived from laboratory experiments on the circular cylinder and then were applied to the square section, for which the VIV-galloping model was developed. The proper characterization of these parameters would require force measurements on spinning cylinders (see Ref. [24] for preliminary test results in a water channel) and flow visualizations in the near wake of the section with the side ratio of interest.

Table 4. Nominal values of the unsteady parameters set in Tamura and Shimada's model.

f	h^*	C_{L0}	St
1.16	1.8	0.656	0.106

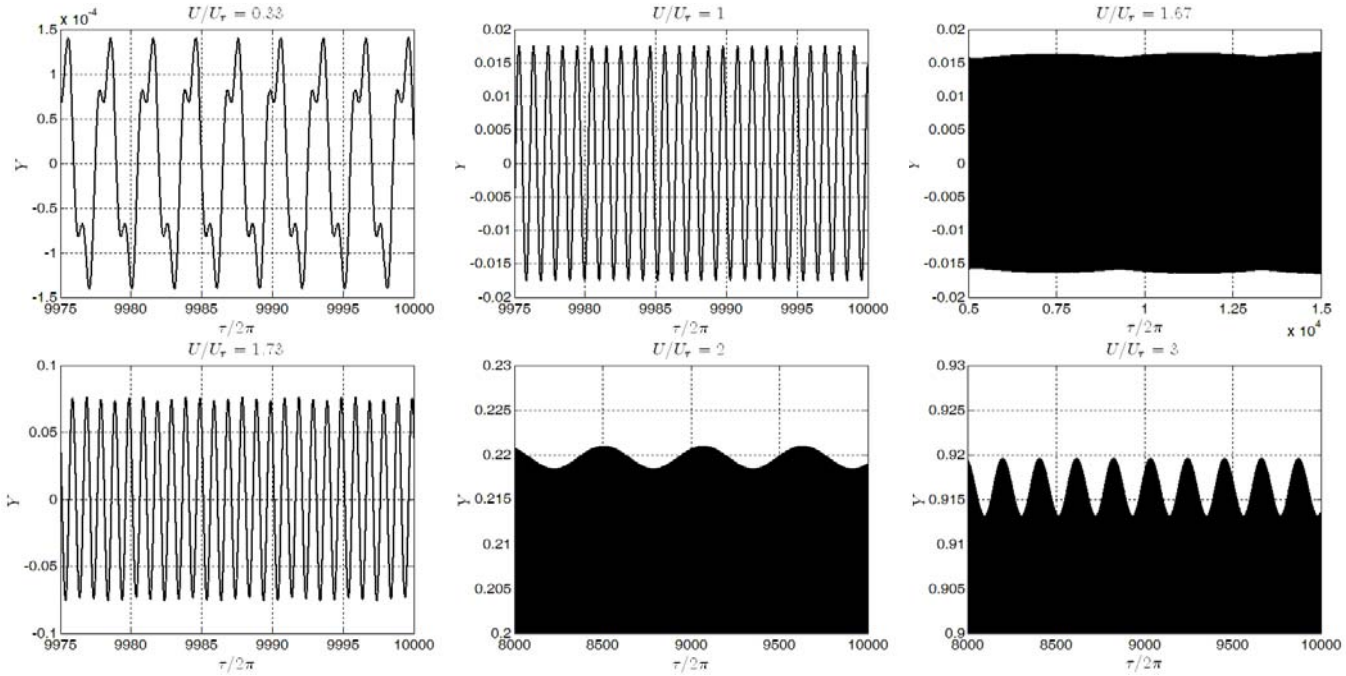

Figure 20. Time histories of nondimensional displacement obtained in the numerical simulations for test case #3 (Sc = 28.0) with nominal values of the model parameters for various reduced wind speeds.

First, let us examine the results obtained for test case #6, which is relative to a value of the Scruton number (Sc = 87.7) promoting no interference between VIV and galloping. Figure 21 shows that, also in this case, the response amplitudes are underestimated by using the nominal reference values of the parameters. The resonance onset is generally well predicted and the h^* parameter does not seem to affect the response. By contrast, f and C_{L0} have a similar effect in amplifying the response amplitude when doubled, so to better reproduce the experimentally observed results. Nevertheless, while increasing C_{L0}, the maximum peak of the resonance response curve is fixed to a value slightly smaller than U/U_r = 1, instead of being correctly shifted to higher reduced velocity values, as it is for the parameter f. A value of f around 4.64 (four times the nominal value f = 1.16) resulted to give the best accordance in terms of peak value of the resonance response, while a value of 9.28 is even better in reproducing the slope of the growing branch of the response, with only a small overestimation of the peak magnitude. The latter also entails a moderate increase in the width of the resonance curve. It is clear that f plays a role similar to that of the parameter c in Corless and Parkinson's model.

Test case #1 is related to the lowest Scruton number tested (Sc = 2.9) and consequently to the minimum theoretical quasi-steady galloping critical wind speed (U_g/U_r = 0.19). Asynchronous quenching occurs in this case, in the sense that vortex shedding is able to prevent galloping instability up to the resonance flow velocity (*e.g.* Ref. [1]). In fact, the experimental curve presents a secondary resonance at $U_r/3$, followed by a post critical galloping branch starting at U_r. Figure 22 reports the results of a sensitivity study on the three model parameters. The response is not significantly affected by either C_{L0} or h^* (apart from small differences in the primary and secondary excitation branches respectively for h^* = 0.9 and h^*= 3.6). Conversely, by changing f some difference in amplitude is apparent in all the response curves around and immediately after the resonance wind speed. In particular, it is extremely interesting the fact that, for a value of f equal to eight times the reference nominal value, that is f = 9.28, the model is able to reproduce not only the onset but also the nearly linear development of the response in amplitude exhibited by the wind tunnel data, although with a much higher slope.

The f variation also puts in light that the onset of the secondary resonance is reasonably well predicted by the calculations and the peak amplitudes strongly depend on the value set for this parameter. The results confirmed those obtained in Ref. [7] for the square cylinder, that a low reduced wind speed excitation is possible for low values of f. For the reference nominal value f = 1.16, the significance of the secondary excitation is overestimated by a factor of about 2, while the amplitude is well predicted for f = 1.60 (although the oscillations do not die out as sudden as in the experiments). Nevertheless, no secondary excitation is predicted for f values larger than two times the assumed nominal value. Also, the effect of increasing f is to separate the secondary resonance from the main instability. The opposite effect was observed for a reduction of the parameter, since the width of the secondary resonance grows up to almost reaching the main instability branch starting at resonance. Nevertheless, as evidenced in the figure, this trend comes to saturation for a value of f equal roughly to one fourth of the nominal value (f = 0.29), given that for a further reduction (f = 0.14) the response curve retraces roughly the previous one. Figure 23 shows that a delay of the secondary excitation onset velocity is produced by an increase of the Scruton number, as previously noted also for Corless and Parkinson's model (Figure 15).

Figure 24 shows the results of the sensitivity study for three values of the Scruton number, focusing on the parameter f. The results for the other two model parameters (C_{L0} or h^*) are not reported here for the sake of brevity, as they only showed a minimal

effect on the amplitude of the response at resonance. Concerning test cases #2 and #3 (Figure 24a-b), for such different values of the Scruton number (5.1 and 28.0) the experimental responses differ only for the presence or not of the secondary resonance. Beyond the vortex-resonance critical velocity, the response amplitudes predicted by the analytical model significantly overestimates the experimental data, although $f = 9.28$ gives again the best result.

The transition from test case #2 to #3 in Figure 24b is representative of a quasi-steady galloping critical velocity nearly six times larger in the second case ($U_g/U_r = 1.86$ instead of 0.34). This value still allows the interference between the two phenomena, as demonstrated by the present experimental results and literature evidences (Refs. [1-3]). Nevertheless, in the analytical modelling the separation between the resonance region and the galloping branch is obtained for the nominal value assumed for f. In fact, for $f \leq 1.16$ clear separation between the two excitation mechanisms takes place, although the onset velocity for galloping instability is slightly lower than the theoretical quasi-steady value. By reducing f, a significant decrease of the amplitude in the resonance region is observed and for a value of 0.29 the amplitudes nearly vanish in the neighborhood of $U/U_r = 1$. By setting the value of f to 2.32 and 4.64 (two and three times the nominal value) respectively for test case #3 and #4, for initial conditions $Y(0) = 0.01$, $Y'(0) = 0$, the vibration amplitudes drop to lower values after the resonance region ($1.30 < U/U_r < 1.75$ in Figure 24b and $1.50 < U/U_r < 2.25$ in Figure 24c), close to those observed in the experiments. By starting the calculations from high-amplitude initial conditions, namely $Y(0) = 15° \cdot \pi/180 \cdot V_{red}$, $Y'(0) = 0$, the branch connecting the resonance and the galloping regions slightly shrinks. A pair of hysteresis loops are indeed apparent. By increasing the value of f to 4.64, a full interference between VIV and galloping is predicted, although the experimental results are significantly overestimated. Once more, a value of the parameter f equal to eight times the nominal one gives a much improved result, even better than in test case #2. By looking at Figure 24c, relative to test case #4, it is apparent an overall scenario quite close to test case #3, except for the fact that the same behavior obtained with $f = 2.32$ for test case #3 is reproduced for test case #4 by setting $f = 4.64$. It is important to notice that the nearly linear trend of the experimental amplitude-velocity curve is fairly well approximated in this case. A value $f = 8.0$ was also considered with the aim of trying to refine the results and it can be concluded that the highest considered value of f gives the best result.

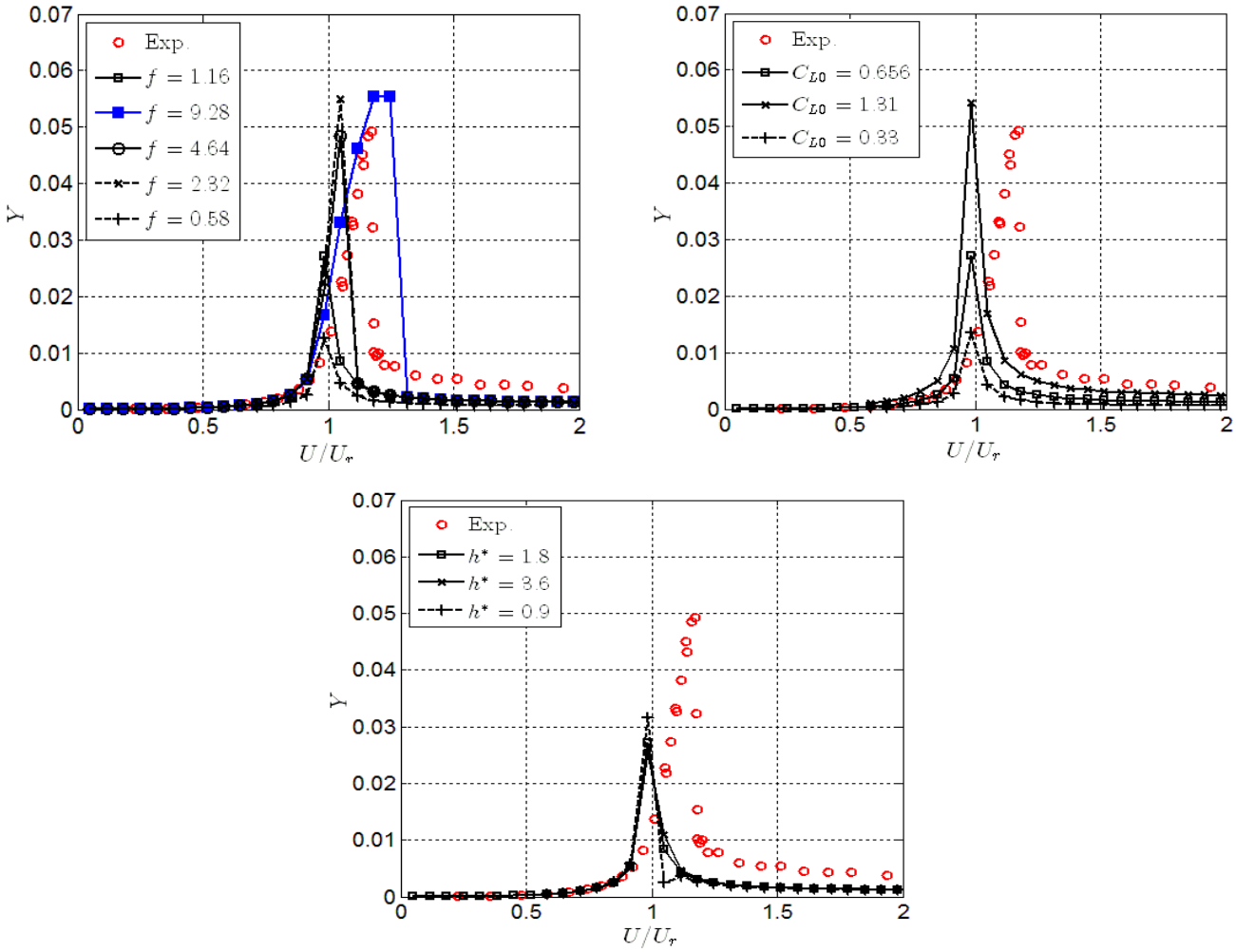

Figure 21. Comparison between experimental and numerical results obtained with Tamura and Shimada's model for $Sc = 87.7$ (test case #6).

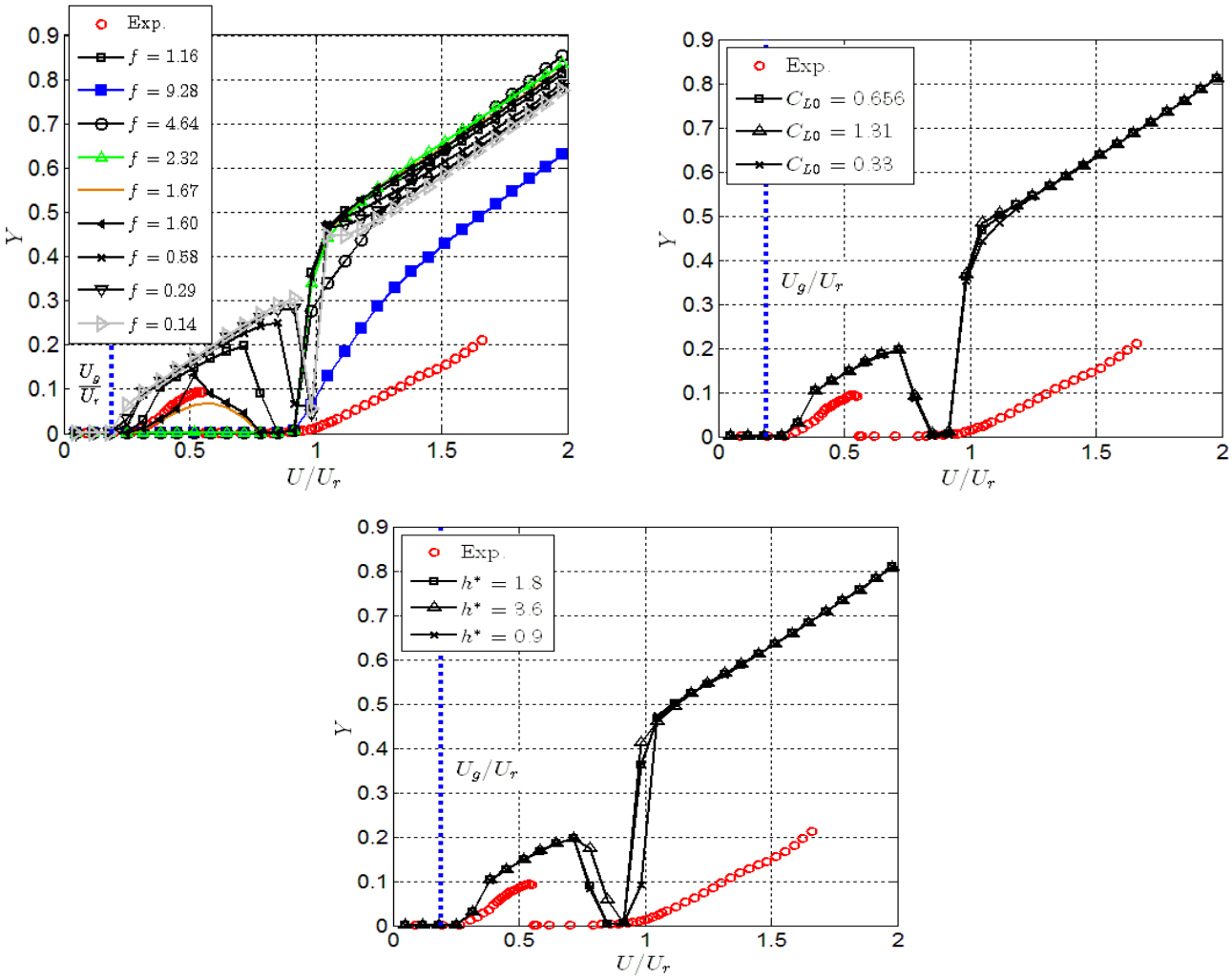

Figure 22. Comparison between experimental and numerical results obtained with Tamura and Shimada's model for $Sc = 2.9$ (test case #1). The dashed line indicates the ratio of quasi-steady galloping critical velocity to vortex-resonance velocity.

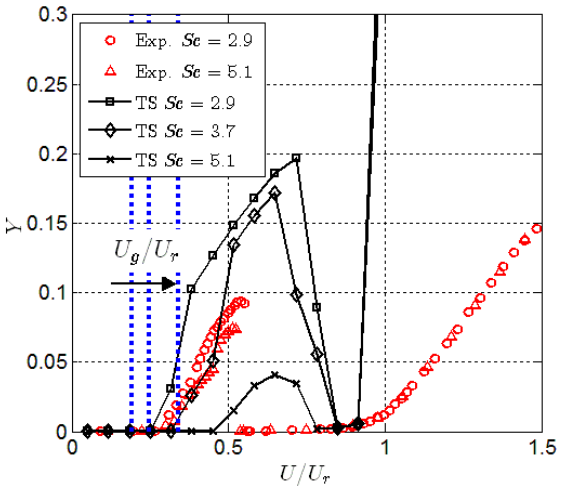

Figure 23. Comparison between experimental and numerical results obtained with Tamura and Shimada's model (TS) for three different Scruton numbers.

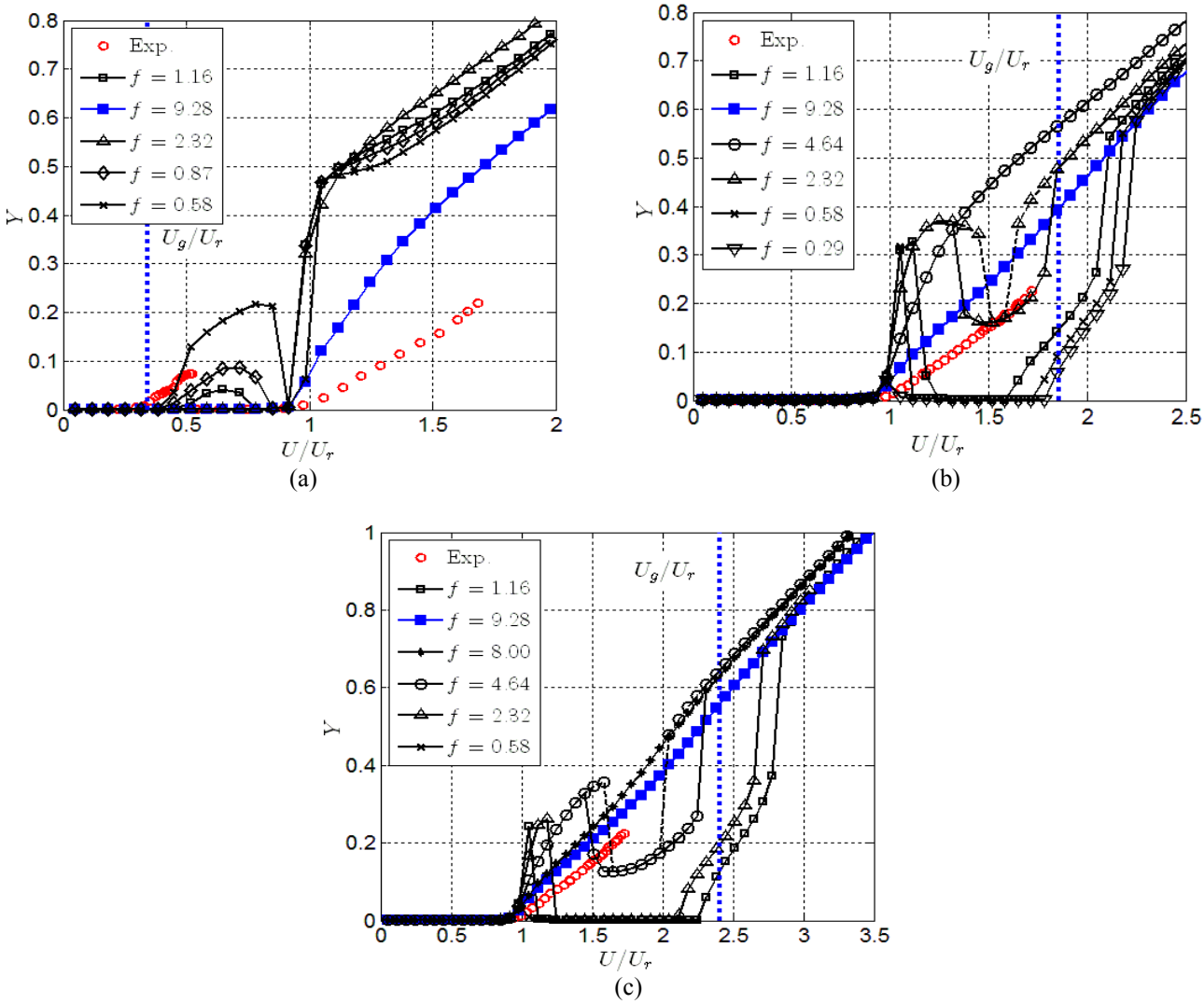

Figure 24. Sensitivity study conducted on f parameter of Tamura and Shimada's model for case #2 (Sc = 5.1, top-left, frame a), case #3 (Sc = 28.0, top-right, frame b) and case #4 (Sc = 36.2, bottom, frame c). Solid and dashed lines indicate respectively solutions obtained from initial conditions $Y(0) = 0.01$, $Y'(0) = 0$ and from $Y(0) = 15° \cdot \pi/180 \cdot V_{red}$, $Y'(0) = 0$.

5 CONCLUDING REMARKS

The models of interference between vortex-induced vibration and galloping instability available in literature were discussed in the first part of the paper. Then, Corless and Parkinson's and Tamura and Shimada's models were applied to the case of a rectangular cylinder with a side ratio of 1.5 elastically suspended in a smooth air flow, which was tested in the wind tunnel by the authors. An extensive sensitivity study on the parameters appearing in the model equations was also carried out.

The main conclusions of the present investigation are summarized here:

- Both models rely on the principle that the unsteady forces responsible for vortex-induced vibration and the quasi-steady forces producing galloping can simply be added. Moreover, although quasi-steady forces are supposed to apply only for high reduced flow speed, these models use them without any modification also in the resonance range and therefore for very low reduced wind speed.
- The crucial equation parameters are those denoted as c for Corless and Parkinson's and f for Tamura and Shimada's model.
- Both models are able to satisfactorily reproduce the pure VIV excitation with moderate amplitudes observed in the experiments for high values of the Scruton number, if relatively high values of c and f are set in the equations (about four times larger than those assumed in the original analyses for the square cylinder).
- With this or lower values of c, Corless and Parkinson's model fails to predict significant VIV-galloping interference for high values of the Scruton number. For lower Scruton numbers, a combined instability is obtained but the numerical results significantly overpredicts the amplitude of oscillation around the resonance region.
- The behavior of Tamura and Shimada's model is similar but an even higher value of f (eight times the nominal value f = 1.16) allows to reproduce with acceptable accuracy the nearly linear increase of the oscillation amplitude with the wind speed

beyond the vortex-resonance threshold observed in the experiments. Such a behavior was not observed with Corless and Parkinson's model, not even for very high values of *c*.

- For low Scruton numbers, both models are able to feature the secondary excitation starting in the experiments around a wind speed equal to one third of the vortex-resonance one. Nevertheless, this is possible only for small values of the parameters *c* and *f*. In addition, the left limit of the range of this low-speed excitation was not dependent on the Scruton number in the experiments, while it was in the numerical simulations.

Finally, despite their theoretical limits, the models studied are able to reproduce some interesting features of the complex phenomenon of VIV-galloping interference observed in the wind tunnel tests. Therefore, a future effort to further explore and improve them, and in particular Tamura and Shimada's model, is doubtless worth.

REFERENCES

[1] C. Mannini, A.M. Marra and G. Bartoli, VIV-galloping instability of rectangular cylinders: Review and new experiments, *Journal of Wind Engineering and Industrial Aerodynamics* 132, 109-124, 2014.

[2] C. Mannini, A.M. Marra and G. Bartoli, Experimental investigation on VIV-galloping interaction of a rectangular 3:2 cylinder, *Meccanica* 50 (3), 841-853, 2015.

[3] C. Mannini, A.M. Marra, T. Massai and G. Bartoli, VIV-galloping instability of a rectangular cylinder in turbulent flow, *Proceedings of the 14th International Conference on Wind Engineering*, Porto Alegre, Brazil, 2015.

[4] T.V. Santosham, *Force measurements on bluff cylinders and aeroelastic galloping of a rectangular cylinder*, M.Sc. thesis, Vancouver, Canada, University of British Columbia, 1966.

[5] D.N. Bouclin, *Hydroelastic oscillations of square cylinders*, M.Sc. thesis, Vancouver, Canada, University of British Columbia, 1977.

[6] R.M. Corless and G.V. Parkinson, A model of the combined effects of vortex-induced oscillation and galloping, *Journal of Fluids and Structures* 2 (3), 203-220, 1988.

[7] Y. Tamura and K. Shimada, A mathematical model for the transverse oscillations of square cylinders, *Proceedings of the 1st International Conference on Flow Induced Vibrations*, Bowness-on-Windermere, UK, Springer-Verlag, pp. 267-276, 1987.

[8] G.V. Parkinson and N.P.H. Brooks, On the aeroelastic instability of bluff cylinders, *Journal of Applied Mechanics* 28 (2), 252-258, 1961.

[9] G.V. Parkinson and J.D. Smith, The square prism as an aeroelastic non-linear oscillator, *Quarterly Journal of Mechanics and Applied Mathematics* 17 (2), 225-239, 1964.

[10] R.T. Hartlen and I.G. Currie, Lift-oscillator model of vortex-induced vibration, *Journal of Engineering Mechanics Division* 96 (5), 577-591, 1970.

[11] R.M. Corless and G.V. Parkinson, A model of the combined effects of vortex-induced vibration and galloping: Part II, *Journal of Fluids and Structures* 7 (8), 825-848, 1993.

[12] P.W. Bearman, I.S. Gartshore, D.J. Maull and G.V. Parkinson, Experiments on fluid-induced vibration of a square-section cylinder, *Journal of Fluids and Structures* 1 (1), 19-34, 1987.

[13] Y. Tamura and G. Matsui, Wake-oscillator model of vortex-induced oscillation of circular cylinder, *Proceedings of the 5th International Conference on Wind Engineering*, Forth Collins, US, Elsevier, pp. 1085-1094, 1979.

[14] Y. Tamura and A. Amano, Mathematical model for vortex-induced oscillations of continuous systems with circular cross section, *Journal of Wind Engineering and Industrial Aerodynamics* 14 (1-3), 431-442, 1983.

[15] G. Birkhoff, Formation of vortex streets, *Journal of Applied Physics* 24 (1), 98-103, 1953.

[16] M. Funakawa, Excitation mechanism of an elastically supported circular cylinder in a flowing fluid, *Bulletin of Japan Society of Mechanical Engineers* 35 (270), 303-312, 1969 (in Japanese).

[17] Y. Nakamura, Vortex excitation of a circular cylinder treated as a binary flutter, *Reports of Research Institute for Applied Mechanics* 17 (59), 217-234, 1969.

[18] M.A. Wawzonek, *Aeroelastic behavior of square section prisms in uniform flow*, M.Sc. thesis, Vancouver, Canada, University of British Columbia, 1979.

[19] C. Mannini, A.M. Marra, T. Massai and G. Bartoli, Aeroelastic instabilities of rectangular cylinders with various side ratios, *Proceedings of the 13th Conference of the Italian Association for Wind Engineering*, Genoa, Italy, 2014.

[20] A. Barrero-Gil, A. Sanz-Andrés, G. Alonso, Hysteresis in transverse galloping: The role of the inflection points, *Journal of Fluids and Structures* 25 (6), 1007-1020, 2009.

[21] A. Luongo, D. Zulli, Parametric, external and self-excitation of a tower under turbulent wind flow, *Journal of Sound and Vibration* 330 (13), 3057-3069, 2011.

[22] I. Kirrou, L. Mokni, M. Belhaq, On the quasiperiodic galloping of a wind-excited tower, *Journal of Sound and Vibration* 332 (18), 4059-4066, 2013.

[23] I. Kirrou, L. Mokni, M. Belhaq, Quasiperiodic galloping of a wind-excited tower near secondary resonances of order 2, *Journal of Vibration and Control* (in press).

[24] T. Massai, *On the interaction between vortex-induced vibrations and galloping in rectangular cylinders of low side ratio*, Ph.D. thesis, University of Florence, Italy – TU Braunschweig, Germany, 2015.